Computational study of the impacts of mechanical and physical cell properties on mitotic cell rounding in developing epithelia

Ali Nematbakhsh[a,†]; Wenzhao Sun[a,†]; Pavel A. Brodskiy[b,†]; Aboutaleb Amiri[c]; Cody Narciso[b]; Zhiliang Xu[a]; Jeremiah J. Zartman[b,*]; Mark Alber[a,d,*]

[a] Department of Applied and Computational Mathematics and Statistics, University of Notre Dame, Notre Dame, IN 46556, USA

[b] Department of Chemical and Biomolecular Engineering, University of Notre Dame, Notre Dame, IN 46556, USA

[c] Department of Physics, University of Notre Dame, Notre Dame, IN 46556, USA

[d] Department of Mathematics, University of California, Riverside, CA 92521, USA

[†] Equal contribution.

[*] Corresponding authors: malber@nd.edu (M. Alber) and jzartman@nd.edu (J.J. Zartman)

Abstract

Mitotic rounding (MR) during cell division is critical for the robust segregation of chromosomes into daughter cells and is frequently perturbed in cancerous cells. MR has been studied extensively in individual cultured cells, but the physical mechanisms regulating MR in intact tissues are still poorly understood. A cell undergoes mitotic rounding by simultaneously reducing adhesion with its neighbors, increasing actomyosin contraction around the cortex, and increasing the osmotic pressure of the cytoplasm. Whether these changes are purely additive, synergistic or impact separate aspects of MR is not clear. Specific modulation of these processes in dividing cells within a tissue is experimentally challenging, because of off-target effects and the difficulty of targeting only dividing cells. In this study, we analyze MR in epithelial cells by using a newly developed multi-scale, cell-based computational model that is calibrated using experimental observations from a model system of epithelial tissue growth, the *Drosophila* wing imaginal disc. The model simulations predict that increase in apical surface area of mitotic cells is solely driven by increasing cytoplasmic pressure. MR however is not achieved within biological constraints unless all three properties (cell-cell adhesion, cortical stiffness and pressure) are simultaneously regulated by the cell. The new multi-scale model is computationally implemented using a parallelization algorithm on a cluster of graphic processing units (GPUs) to make simulations of tissues with a large number of cells feasible. The model is extensible to investigate a wide range of cellular phenomena at the tissue scale.

Author Summary

Mitotic rounding (MR) during cell division is critical for the robust segregation of chromosomes into daughter cells and is frequently perturbed in cancerous cells. MR has been studied extensively in individual cultured cells, but the physical mechanisms regulating MR in intact tissues are still poorly understood. The newly developed computational model Epi-scale enables one to produce new hypotheses about the underlying biophysical mechanisms governing MR of epithelial cells within the developing tissue micro-environment. In particular, our simulations results predict that robust mitotic rounding requires co-current changes in cell-cell adhesion, cortical stiffness and cytoplasmic pressure, and explains how regulation of each property impacts the shapes of dividing cells in tissues.

Introduction

Epithelia are tissues composed of tightly adherent cells that provide barriers between internal cells of organs and the environment and are one of the four basic tissue types in the human body [1–3] (Fig. 1). Epithelial expansion driven by cell proliferation is a key feature throughout development, and it also occurs in hyperplasia, a precursor to cancer. Cell divisions during development must occur robustly, as mis-segregation of chromosomes leads to severe genetic abnormalities (aneuploidy) in daughter cells. Over 90% of all human tumors are epithelially-derived [4], and the accumulation of genetic errors during cell division can lead to all of the hallmarks of cancer [5]. In tissues, mitotic cells must become sufficiently round to avoid the mis-segregation of chromosomes all the while still remaining connected with their neighbors [6]. A deeper understanding of the biophysical mechanisms governing the behavior of mitotic cells in epithelia will result in a better understanding of many diseases including cancer.

Epithelial cells entering mitosis rapidly undergo structural changes that result in the apical area of the cell becoming larger and rounder, in a process known as mitotic rounding (MR) [7,8]. MR occurs in detached cells, cells adherent to a substrate as well as in epithelial cells within tissues [9–11]. The beginning of MR in epithelia coincides with an increased polymerization of actomyosin at the cell cortex, which results in an increase in cortical tension and is necessary for MR [10,12]. Simultaneously, intracellular pressure increases [10], and cells partially reduce adhesion to their neighbors and the substrate [12]. Experiments that can specifically target only dividing

77 cells and measure physical properties of individual cells within tissues are very
78 challenging.
79
80 Computational modeling coupled with experimentation has become a powerful tool for
81 identifying the biophysical principles governing organogenesis [13]. Biophysically-
82 derived computational models can complement current experimental methods by
83 predicting the response of tissue to mechanical perturbations of individual cells. MR is
84 investigated in this paper by using a novel multi-scale sub-cellular element model (SEM)
85 called Epi-scale that simulates epithelial cells in growing tissues. Novel biologically-
86 relevant features of the model include: i) separate representations of the sub-cellular
87 elements, as well as cell-cell interactions; ii) a detailed description of cell properties
88 during mitotic rounding; and iii) a systematic calibration of model parameters to provide
89 accurate biological simulations of tissue growth. We performed parameter sweeps on
90 the extent that a mitotic cell regulates cell-cell adhesion, membrane stiffness, or internal
91 pressure and analyzed the impacts of such parameter variations on cross-sectional
92 areas of mitotic cells at the apical surface as well as the roundness of mitotic cells.
93
94 Model simulations demonstrate that cell-cell adhesion and stiffness significantly impact
95 roundness but do not increase cell area during MR. Solely increasing cell pressure
96 during MR increases both cell area and roundness. However, the internal pressure
97 increase needed to achieve experimentally observed levels of roundness leads to
98 nonphysical levels of cell area expansion (Fig. S5). The model predicts that a cell must

regulate all three cellular properties simultaneously to achieve physiological levels of area expansion and roundness without adversely affecting tissue integrity.

The paper is organized as follows. The Methods section describes the modeling background and model development. The Results section provides details of model calibration of single cell parameters using quantitative biophysical data. The calibrated model predicts emergent properties of epithelial topology. The model is then used to investigate new questions into the relative contributions of cell-cell adhesion, membrane stiffness and intracellular pressure impact the extent of mitotic rounding. The paper ends with a detailed discussion of the models' predictions in the more general biological context. It also describes future extensions of the computational model environment, for simulating epithelial tissue mechanics in greater biological detail.

Methods

Modeling background

Multiple computational approaches have been utilized to model various aspects of epithelial tissue dynamics, each with its particular focus and applications [14]. For example, the cellular Potts modeling (CPM) approach has been used successfully to take into account cell adhesivity to study cell aggregation as well as cell morphogenesis [15,16]. Finite element models (FEMs) have also been implemented to investigate epithelial cell behavior [17,18]. Vertex based models (VBM) provided an efficient approach to study the regulation of cell topology, tissue-size regulation, tissue morphogenesis, and the role of cell contractility in determining tissue curvature [19–24].

Cells are defined in VBMs by the several vertices representing the meeting points of shared cell-cell contacts (as reviewed in [19]). An implementation and comparison of the five popular cell-based modelling approaches for simulating the self-organization of multicellular tissues within a consistent computational framework, Chaste [25] (http://www.cs.ox.ac.uk/chaste), was recently described in [26].

The Subcellular Elements Model (SEM), developed initially by Newman's group [27] for simulating multi-cellular systems to encompass multiple length scales, is currently actively used as a general computational modeling approach. SEMs have been extended to predict how mechanical forces generated by cells are redistributed in a tissue and for studying tissue rheology, tissue fusion, thrombus formation, and cell-cell signaling. SEM was also used to study aspects of epithelial cell mechanics without making assumptions about cell shapes [28]. Each cell in a SEM consists of a set of nodes representing a coarse-grained representation of subcellular components of biological cells. Node-node interactions are represented by energy potentials. Another SEM developed by Jamali et al. [29] represents the membrane and nucleus of the cell by nodes connected by overdamped springs. Gardiner et al. [30] described a SEM with locally-defined mechanical properties. Christely et al. [31] have developed an efficient computational implementation of the SEM simulating role of Notch signaling in cell growth and division, on GPU cluster to decrease computational time. A particular advantage of the SEM approach is that it can provide local representations of mechanical properties of individual cells which can be directly related to the experimental data [32].

The Epi-scale computational model

This paper represents detailed simulations obtained using novel multi-scale SEM called Epi-scale, of developing epithelia with a focus on the two-dimensional (2D) planar cell shapes near the apical surfaces of cells. This is a simplifying approximation that was used in many previous models of wing disc growth [22,23,33–35]. In particular, it is reasonable to use a 2D model for studying many epithelial processes in the *Drosophila* wing disc pouch because it consists of a single layer of cells and the essential structural components of those cells, including E-cadherins and actomyosin, are concentrated on the apical surface of the epithelia (Fig. 1c-d). E-cadherin is responsible for adhesion between two neighboring cells, and actomyosin, which is concentrated at the apical MR drives cell contractility. The nucleus and most of the cytoplasm are pushed up to the apical surface during cell division. Using a 2D approximation also allows us to model a large number of cells with high resolution and special attention to mechanical cell properties. However, future development of the Epi-scale simulation platform implemented on GPU clusters, will also enable 3D simulations with reasonable computational costs.

In what follows, we first describe different types of the subcellular elements that are used to simulate each cell, and the interactions between them. Then, the equations of motion of each subcellular element are provided. Finally, approaches for modeling cell's growth, transition to mitotic phase, and division are described.

Subcellular elements

169 Epi-scale represents individual cells as collections of two types of interacting subcellular
170 elements: internal nodes and membrane nodes (Fig. 2). The internal nodes account for
171 the cytoplasm of the cell, and the membrane nodes represent both plasma membrane
172 and associated contractile actomyosin cortex. The internal and membrane nodes are
173 placed on a 2D plane, representing the apical surface of epithelia.
174
175 Interactions between internal and membrane nodes are modeled using potential energy
176 functions as shown in Fig. 2a [31,36]. The internal–internal nodes interactions represent
177 the cytoplasmic pressure of a cell, and the interactions between membrane nodes of the
178 same cell are used to model the cortical stiffness. Cell-cell adhesion is modeled by
179 membrane-membrane nodes interactions between two neighboring cells. List of all
180 potential functions used in the Epi-scale to model mechanical properties of cells and
181 epithelial tissue and description of their biological relevance are provided in Table 1.
182
183 Epi-scale utilizes spring and Morse potential functions. Linear and torsional springs are
184 used for modeling interactions E_{ik}^{MMS} and E_{i}^{adh}, while Morse potential functions are used
185 for modeling interactions E_{ij}^{MI}, E_{ik}^{II}, and $E_{\alpha_i}^{MMD}$ (Fig. 2). Morse potential consists of two
186 terms, generating short-range repulsive and long-range attractive forces [27]. The
187 following expression is a Morse potential function for the E_{ij}^{MI}:
188

$$E_{ij}^{MI} = \left[U^{MI} \exp\left(-\frac{\left| \boldsymbol{x_i} - \boldsymbol{x_j} \right|}{\xi^{MI}} \right) - W^{MI} \exp\left(-\frac{\left| \boldsymbol{x_i} - \boldsymbol{x_j} \right|}{\gamma^{MI}} \right) \right] \quad (1)$$

189

where U^{MI}, W^{MI}, ξ^{MI}, and γ^{MI} are Morse parameters for the E_{ij}^{MI} which are carefully calibrated using specific experimental data. The same form of the potential with different sets of parameters is also used for E_{ij}^{MI} and E_{il}^{MMD} (Table 2). These potential functions govern the motion of internal and membrane nodes inside the cells resulting in the deformation and rearrangement of cells within the tissue.

Equations of motion

Equations of motion differ for membrane nodes and internal nodes. For each internal or membrane node and at each time-point, displacement of a subcellular element is calculated based on the potential energy functions. The model assumes that nodes are in an overdamped regime [22,36,37] so that inertia forces acting on the nodes can be neglected. This leads to the following equations of motion describing movements of membrane and internal nodes, respectively:

$$\eta \dot{\boldsymbol{x}}_i^I = -\left(\sum_j \nabla E_{ij}^{MI} + \sum_m \nabla E_{im}^{II} \right) \qquad i = 1,2,\ldots..N^I \tag{2}$$

$$\eta \dot{\boldsymbol{x}}_j^M = -\left(\sum_i \nabla E_{ij}^{MI} + \sum_k \nabla E_{kj}^{MMS} + \sum_l \nabla E_{lj}^{MMD} + \nabla E_j^{adh} \right) \qquad j = 1,2,..N^M \tag{3}$$

where η is the damping coefficient, $\boldsymbol{x}_i^M$ and $\boldsymbol{x}_j^{\boldsymbol{M}}$ are positions of internal and membrane nodes, respectively. The dot represents a time derivative.

Eqns. (2) and (3) are discretized in time using forward Euler method and positions of nodes $\boldsymbol{x}_{\boldsymbol{I}_i}$ and $\boldsymbol{x}_{\boldsymbol{M}_i}$ are incremented at discrete times. The forward Euler discretization of the equation of motion of internal nodes (Eqn. (2)) has the form:

$$\boldsymbol{x}_i^I\,(\mathrm{t}+\Delta\mathrm{t}) = \boldsymbol{x}_i^I\,(\mathrm{t}) - \left(\sum_j \nabla\left(E_{ij}^{II}\right)(\mathrm{t}) + \sum_k \nabla\left(E_{\alpha_{ik}}^{MI}\right)(t)\right)\frac{\Delta t}{\eta} \tag{4}$$

where Δt is the time step size. The same discretization technique is used for the equation of motion of the membrane nodes.

The Epi-scale was computationally implemented on the cluster of Graphical Processing Units (GPUs). This enabled us to run large number of simulations with subcellular resolution at micro-scale with low computational cost and to study the impact of changes in individual cell physical properties on the tissue development at the macro-scale. (See Supplementary Information (SI-S1) for details.)

Cell cycle

The *Drosophila* wing disc, which was used for calibrating the model, has a spatially uniform growth rate which decreases over time [38]. The growth rate for cell *ii* is modeled by an exponentially decaying function fit to the specific experimental data [38], with a random term representing stochastic variation among cells:

$$g_{ii}(t) = (g_{0_{Avg}} + Rnd[-g_0, g_0])e^{-k_g t} \tag{5}$$

where $g_{0_{Avg}}$ is the average growth rate of cells in the beginning of a simulation and $Rnd[-g_0, g_0]$ is a random number chosen from a uniform distribution in the range $[-g_0, g_0]$. k_g is the decay constant of the growth rate.

Cells evolve through interphase and mitosis phases. Variable Cell Progress ($CP \in [0,1]$) describes in the model cell's progress between the beginning of the interphase ($CP = 0$) to the end of the cell division ($CP = 1$). CP is updated based on cell's growth rate as follows:

$$CP_{ii}(\mathrm{t} + \Delta t) = CP_{ii}(\mathrm{t}) + g_{ii}(\mathrm{t}) \cdot \Delta t \quad (6)$$

The number of internal nodes inside the cell increases as the cell grows (Fig. 2). It has been shown experimentally that epithelial cells undergoing mitosis increase their intracellular pressure by adjusting their osmolarity relative to their surroundings [39]. Additionally, the actomyosin cortex is enriched, and cellular adhesion to the substrate and to neighboring cells are downregulated [10,40–44]. Since these changes in mitotic cells occur concurrently, the relative impact on mitotic cells cannot easily be decomposed into separable effects in experiments.

To simulate MR, parameters regulating cell-cell adhesion, actomyosin cortex, and internal pressure of cells in the mitotic phase (M phase) are modified (Table 2), representing changes of cell physical properties during mitosis [9,10,43]. Mitosis is

modeled by a linear transition from the interphase parameter range to the mitotic parameter range determined based on the experimental observations. For example U^{MI}, a Morse parameter used for representing cytoplasmic pressure on the membrane of the cell (see SI-S2.3), is varied from the interphase value (U^{MI}_{Inter}) to the mitotic value (U^{MI}_{Mit}), by using the following function of *CP*:

$$U^{MI} = U^{MI}_{Inter}\frac{1 - CP}{1 - CP_{Mit}} + U^{MI}_{Mit}\frac{CP - CP_{Mit}}{1 - CP_{Mit}} \quad (7)$$

where U^{II}_{Mit} is the parameter value in the mitosis range. Similar linear variations of parameter values are used for representing enrichment of actomyosin cortex and reduction in cell-cell adhesion with neighboring cells in mitotic phase (see Table 1).

Cells in the mitotic (M) phase – which lasts approximately 30 minutes – divide into two daughter cells (Fig. 2). As *CP* becomes equal to 1, cytokinesis occurs that is modeled by separating internal and membrane elements of the mother cell into two sets representing daughter cells. The axis of division is implemented perpendicular to the cell's longest axis, following Hertwig's rule [45]. New membrane elements are created along the cleavage plane for each daughter cell, and cell parameters for nodes of each daughter cell are set to values from the interphase range and *CP* is reset to zero for both daughter cells.

Membrane nodes in the beginning of a simulation are arranged in a circle for each cell, and internal nodes randomly placed within each cell (Fig. 3a). After initialization, internal

nodes rapidly rearrange in a simulation, and cells self-organize into a polygonal network, similar to the experimentally observed cell packing geometry of epithelia (Fig. 3b). Cells constantly grow, divide and interact with each other resulting in a detailed simulation of the developing epithelial tissue (Fig. 3c-d).

Results

Model Calibration

Before running predictive model simulations, the model parameters, described in the Epi-scale computational model section, were calibrated using experimental data for the third instar *Drosophila* wing disc, which is a powerful model for studying organ formation [46,47] (Fig. 4, SI Movie S4.1). Experimental values for epithelial cell lines were used to calibrate the model parameters when experimental data for *Drosophila* wing disc were not available.

Mechanical stiffness of the actomyosin cortex is primarily responsible for the modulus of elasticity (E) and the Poisson's ratio of the cells [48]. E is experimentally obtained by applying known force to either side to stretch a cell, and measuring the cell's deformation based on the applied force [49,50]. This experiment can be reproduced *in silico* by applying forces to membrane nodes on either side of a simulated cell, and measuring the deformation (Fig. 4a-a'', 4c). Parameters corresponding to cortical stiffness (k_{Inter}^{St} and L_{Inter}^{St}) were calibrated to have $E = 19\ kPa$, which is within the biological range of $10 - 55\ kPa$ [49,50] measured for epithelial cells.

The cell-cell adhesive force ($\boldsymbol{F}_{adh}$), or the force needed to detach two adhered cells from each other, is dependent on the strength of cell-cell adhesions. $\boldsymbol{F}_{adh}$ is experimentally obtained by measuring the force needed to detach two adhered cells from each other. This experiment can be reproduced *in silico* by applying forces to membrane nodes on either side of two adhered cells, and measuring the force needed to separate them (Fig. 4b-b"). Parameters corresponding to cell-cell adhesion (k_{Inter}^{adh} and L^{adh}) were calibrated such that $\boldsymbol{F}_{adh} = 20\, nN/\mu m$ (Fig. 4d), which is in the range of experimental results for epithelial MDCK cells [51] and E-Cadherin-transfected S180 cells [52].

Cells in the wing disc have spatially-uniform growth-rates that slow down as the tissue approaches its final size [38]. The growth rate in the Epi-Scale model described by Eqn. (5) was calibrated (Table 3) such that the number of cells in time as the tissue grows follows the experimental data [38] (Fig. 4e). Cells in mitosis deviate from cells in interphase in their area and roundness. The area and roundness of interphase and mitotic cells are calibrated based on the data from the wing disc (Fig. 5e-f). SI-S2.2 provides additional details about the methods used in this study to measure the size and roundness of cells in the imaginal wing disc pouch.

Tissue topology emerges from cell self-organization driven by cellular mechanics

After model calibration, simulations were run to determine whether this cellular-scale calibration was sufficient to recapitulate topological properties of the tissue (Fig. 6) [53,54]. One metric for tissue topology is the distribution of cell neighbor numbers, or

317 polygon class distribution. Based on the simulation results for studying the tissue growth
318 by using the Epi-Scale model, the polygon class distribution approaches steady state
319 after 35 hours (Fig. 5a, 6b). This distribution matches with the ones reported
320 experimentally for the wing disc and other epithelial systems [32] (Fig. 6d) as well as
321 obtained using other computational models for simulating growing tissues such as
322 vertex based model [22].
323
324 Another way to quantify tissue topology is through evaluation of the three laws
325 describing topological relationships: Euler's law, Lewis law, and Aboav-Weaire Law.
326 Euler's law states that, on average, cells forming a packed sheet should be hexagonal
327 [54]. The Lewis law states that cells with more neighbors should have a larger
328 normalized area [55]. The Aboav-Weaire law states that the average polygon class of
329 each cell's neighbors decreases as the cell's polygon class increases [56]. Simulation
330 results obtained using the calibrated model show the average side of cells to be equal
331 to 5.96 which is in a very good agreement with the Euler's law. The model simulations
332 also satisfy two other laws as shown in Fig. 6c.
333
334 **Impacts of adhesion, stiffness, and cytoplasmic pressure on MR**
335 The Epi-scale model is suitable for generating and testing new hypothesis regarding
336 mechanical mechanisms of the MR because it is capable of representing non-polygonal
337 shapes of cells, and parameters representing mechanical cell properties in the model
338 can be directly related to the properties of cells measured in experiments. Simulations
339 were conducted to predict relative contributions of different cell properties to the relative

size (A_{Mit}/A_{Inter}) and roundness (R) of mitotic cells. Cell-cell adhesion, cortical stiffness and internal pressure were individually varied in two sets of simulations (Table 4) to decouple the effects of these properties on the final size and shape of mitotic cells. In the first set (Fig. 6, blue lines), only one of the three properties of mitotic cells is varied in each simulation, while the other two properties are kept constant and equal to interphase values. In the second set of simulations (Fig. 6, black lines), two of the three parameters are set to calibrated values for mitosis. The third parameter under investigation is varied with respect to its calibrated mitotic value. The extent of variation of each parameter ranges from 100% below to 100% higher the calibrated value. Each of these parameter sweeps can be interpreted conceptually as changing the relative degree to which a mitotic cell is regulating each property during the mitotic phase of the cell cycle.

Fig. 7a-c shows that variation of each of these three cell properties considerably affects the roundness of mitotic cells. As seen in Fig. 7a, decreasing only cell-cell adhesion during the M phase increases the roundness of mitotic cells. Increasing the cortical stiffness (Fig. 7b) and the internal pressure (Fig. 7c) will increase the roundness of mitotic cells. The levels of internal pressure needed to achieve “wild type” values of roundness result in unphysical levels of cell areas (SI Movie S4.2) with noticeable incidence of cell-cell rearrangements. Reducing adhesion leads to rounder cells, but only regulating adhesion levels during mitosis would require a complete loss of adhesion (100% below calibrated values) to reach wild-type levels of roundness.

Fig. 7d-f show normalized cross-sectional areas of mitotic cells (A_{Mit}/A_{Inter}) as cell-cell adhesion, cortical stiffness, and the internal pressure are varied. Varying the adhesivity of mitotic cells results in negligible impact on the area of mitotic cells as is evidenced by a flat line (Fig. 7d, blue line). Increasing only the cortical stiffness (Fig. 7e, blue line) slightly decreases the size of mitotic cells, while increasing cytoplasmic pressure significantly increases it (Fig. 7f, blue line). Table 4 provides detailed information on the impact of variation of different cell properties on mitotic cell's roundness and ratio of maximum cross-sectional area during mitosis to area at interphase. The schematic diagram in Fig. 8 recaps the results shown in Fig. 7 and represents the impact of variation of each individual mechanical property on the final size and roundness of mitotic cells. For a cell to be both large and round requires not only modulating internal pressure but also reducing both adhesion and increasing stiffness co-currently.

In summary, the obtained results suggest that increase in cross-sectional area of mitotic cells is solely driven by increasing cytoplasmic pressure. Mitotic roundness however is not achieved within biological constraints unless all three properties (cell-cell adhesion, cortical stiffness and pressure) are simultaneously regulated by the cell. Without concurrent regulation reducing cell-cell adhesion and increasing cortical stiffness, unrealistic high levels of pressure increase would be required to enforce mitotic roundness, resulting in unphysical levels of cell areas.

Discussion

General models for investigating epithelial mechanotransduction, including MR, require coupling of biologically calibrated mechanical components capable of representing non-

386 polygonal cell shapes, and simulating the membranes as well as cytoplasm of individual
387 cells as separate entities. To accomplish this, a novel multi-scale sub-cellular model,
388 called Epi-scale, was developed in this paper for simulating mechanical and adhesive
389 properties of cells in the developing columnar epithelium of the wing disc which consists
390 of a single layer of cells. The model approximates the tissue as a 2D surface since the
391 majority of the contractile and adhesive forces are localized at the apical surface of the
392 epithelium. Parameter ranges for the computational model were obtained by calibrating
393 the model using single cell stretching experiments, double cell stretching experiments,
394 as well as experimentally observed size distributions of cells during mitosis and
395 interphase, and tissue growth rate of *the Drosophila* wing disc. Cell-cell adhesion and
396 cell elasticity were calibrated using experimental data on epithelial tissues. The
397 calibrated model was tested by successfully reproducing emergent properties of
398 developing tissue such as the polygon class distributions.
399
400 Epi-scale enables one to produce new hypotheses about the underlying biophysical
401 mechanisms governing mitotic rounding of epithelial cells within the developing tissue
402 micro-environment. In particular, results of the model simulations predict that robust
403 mitotic rounding requires co-current changes in cell-cell adhesion, cortical stiffness and
404 cytoplasmic pressure. Regulating only one of the cellular properties does not result in
405 the experimentally observed levels of apical areal expansion and degree of mitotic
406 roundness. The individual contributions of changes in these three mechanical properties
407 to the mitotic cell roundness and area were characterized through detailed parameter
408 sensitivity analysis (Fig. 7).

Changes in all three cell properties were shown to contribute to the degree of roundness *in vivo*, but internal pressure was shown to be the primary driver of mitotic cell area increase. Cell properties can be modulated experimentally in tissue as a whole. However, it is currently challenging to target only dividing cells in a tissue. Cell-cell adhesion is dictated by the adhesive interactions of AJs, which can be modulated pharmacokinetically, or through genetic modification of E-cadherin molecules to alter their binding affinities. Cell stiffness can be adjusted by reducing the contractility of the cortex through pharmacological perturbations. Internal pressure of cells is primarily dictated by osmotic channels regulating the flow of water and ions through the cell membrane, and can be adjusted by modulating those channels, or by changing the osmolarity of the media.

The computational model simulations provide insight into the individual contributions of cell properties to MR and can predict the consequences of dysregulation of mitotic cell rounding on the development and homeostasis of epithelial tissues. One experimental approach that could in future be used for testing the model predictions would be to regulate the expression of E-Cadherin, Myosin-II, and osmotic channel antagonists under a Cyclin B promotor, active during mitosis, resulting in modulation only in dividing cells [57,58]. Alternatively, opto-genetic methods could be employed to selectively regulate individual cell properties [59].

Acknowledgements

The authors acknowledge support from the Notre Dame Integrated Imaging Facility and thank members of the Zartman lab for critical feedback on manuscript drafts.

References

1. Gumbiner B. Structure, biochemistry, and assembly of epithelial tight junctions. Am J Physiol - Cell Physiol. 1987;253: C749–C758.

2. Fristrom D. The cellular basis of epithelial morphogenesis. A review. Tissue Cell. 1988;20: 645–690. doi:10.1016/0040-8166(88)90015-8

3. Lecuit T, Lenne P-F. Cell surface mechanics and the control of cell shape, tissue patterns and morphogenesis. Nat Rev Mol Cell Biol. 2007;8: 633–644. doi:10.1038/nrm2222

4. Miller SJ, Lavker RM, Sun T-T. Interpreting epithelial cancer biology in the context of stem cells: tumor properties and therapeutic implications. Biochim Biophys Acta. 2005;1756: 25–52. doi:10.1016/j.bbcan.2005.07.003

5. Hanahan D, Weinberg RA. The Hallmarks of Cancer. Cell. 2000;100: 57–70. doi:10.1016/S0092-8674(00)81683-9

6. Cadart C, Zlotek-Zlotkiewicz E, Le Berre M, Piel M, Matthews HK. Exploring the Function of Cell Shape and Size during Mitosis. Dev Cell. 2014;29: 159–169. doi:10.1016/j.devcel.2014.04.009

7. Strangeways TSP. Observations on the Changes Seen in Living Cells during Growth and Division. Proc R Soc Lond Ser B Contain Pap Biol Character. 1922;94: 137–141.

8. McConnell CH. Mitosis in Hydra. Mitosis in the Ectodermal Epithelio-Muscular Cells of Hydra. Biol Bull. 1933;64: 86–95. doi:10.2307/1537502

9. Sorce B, Escobedo C, Toyoda Y, Stewart MP, Cattin CJ, Newton R, et al. Mitotic cells contract actomyosin cortex and generate pressure to round against or escape epithelial confinement. Nat Commun. 2015;6: 8872. doi:10.1038/ncomms9872

10. Stewart MP, Helenius J, Toyoda Y, Ramanathan SP, Muller DJ, Hyman AA. Hydrostatic pressure and the actomyosin cortex drive mitotic cell rounding. Nature. 2011;469: 226–230. doi:10.1038/nature09642

11. Stewart MP, Toyoda Y, Hyman AA, Müller DJ. Tracking mechanics and volume of globular cells with atomic force microscopy using a constant-height clamp. Nat Protoc. 2012;7: 143–154. doi:10.1038/nprot.2011.434

12. Ramkumar N, Baum B. Coupling changes in cell shape to chromosome segregation. Nat Rev Mol Cell Biol. 2016;advance online publication. doi:10.1038/nrm.2016.75

13. Brodland GW. How computational models can help unlock biological systems. Semin Cell Dev Biol. 2015;47–48: 62–73. doi:10.1016/j.semcdb.2015.07.001

14. Maclaren OJ, Byrne HM, Fletcher AG, Maini PK. Models, measurement and inference in epithelial tissue dynamics. Math Biosci Eng. 2015;12: 1321–1340. doi:10.3934/mbe.2015.12.1321

15. Chen N, Glazier JA, Izaguirre JA, Alber MS. A parallel implementation of the Cellular Potts Model for simulation of cell-based morphogenesis. Comput Phys Commun. 2007;176: 670–681. doi:10.1016/j.cpc.2007.03.007

16. Chaturvedi R, Huang C, Kazmierczak B, Schneider T, Izaguirre JA, Glimm T, et al. On multiscale approaches to three-dimensional modelling of morphogenesis. J R Soc Interface. 2005;2: 237–253. doi:10.1098/rsif.2005.0033

17. Brodland GW, Viens D, Veldhuis JH. A new cell-based FE model for the mechanics of embryonic epithelia. Comput Methods Biomech Biomed Engin. 2007;10: 121–128.

18. Zhao J, Naveed H, Kachalo S, Cao Y, Tian W, Liang J. Dynamic mechanical finite element model of biological cells for studying cellular pattern formation. 2013 35th Annual International Conference of the IEEE Engineering in Medicine and Biology Society (EMBC). 2013. pp. 4517–4520. doi:10.1109/EMBC.2013.6610551

19. Fletcher AG, Osterfield M, Baker RE, Shvartsman SY. Vertex models of epithelial morphogenesis. Biophys J. 2014;106: 2291–2304.

20. Okuda S, Inoue Y, Adachi T. Three-dimensional vertex model for simulating multicellular morphogenesis. Biophys Physicobiology. 2015;12: 13–20.

21. Osterfield M, Du X, Schüpbach T, Wieschaus E, Shvartsman SY. Three-dimensional epithelial morphogenesis in the developing Drosophila egg. Dev Cell. 2013;24: 400–410. doi:10.1016/j.devcel.2013.01.017

22. Farhadifar R, Röper J-C, Aigouy B, Eaton S, Jülicher F. The Influence of Cell Mechanics, Cell-Cell Interactions, and Proliferation on Epithelial Packing. Curr Biol. 2007;17: 2095–2104. doi:10.1016/j.cub.2007.11.049

23. Aegerter-Wilmsen T, Heimlicher MB, Smith AC, Reuille PB de, Smith RS, Aegerter CM, et al. Integrating force-sensing and signaling pathways in a model for the regulation of wing imaginal disc size. Development. 2012;139: 3221–3231. doi:10.1242/dev.082800

24. Jessica CY, Fernandez-Gonzalez R. Quantitative modelling of epithelial morphogenesis: integrating cell mechanics and molecular dynamics. Seminars in Cell & Developmental Biology. Elsevier; 2016. Available: http://www.sciencedirect.com/science/article/pii/S1084952116302348

25. Mirams GR, Arthurs CJ, Bernabeu MO, Bordas R, Cooper J, Corrias A, et al. Chaste: An open source C++ library for computational physiology and biology. PLoS Comput Biol. 2013;9: e1002970. doi:10.1371/journal.pcbi.1002970

26. Osborne JM, Fletcher AG, Pitt-Francis JM, Maini PK, Gavaghan DJ. Comparing individual-based approaches to modelling the self-organization of multicellular tissues. bioRxiv. 2016; 074351.

27. Newman TJ. Modeling Multicellular Structures Using the Subcellular Element Model. In: Anderson DARA, Chaplain PMAJ, Rejniak DKA, editors. Single-Cell-Based Models in Biology and Medicine. Birkhäuser Basel; 2007. pp. 221–239. Available: http://link.springer.com/chapter/10.1007/978-3-7643-8123-3_10

28. Sandersius SA, Weijer CJ, Newman TJ. Emergent cell and tissue dynamics from subcellular modeling of active biomechanical processes. Phys Biol. 2011;8: 045007.

29. Jamali Y, Azimi M, Mofrad MRK. A Sub-Cellular Viscoelastic Model for Cell Population Mechanics. PLOS ONE. 2010;5: e12097. doi:10.1371/journal.pone.0012097

30. Gardiner BS, Wong KK, Joldes GR, Rich AJ, Tan CW, Burgess AW, et al. Discrete element framework for modelling extracellular matrix, deformable cells and subcellular components. PLoS Comput Biol. 2015;11: e1004544.

31. Christley S, Lee B, Dai X, Nie Q. Integrative multicellular biological modeling: a case study of 3D epidermal development using GPU algorithms. BMC Syst Biol. 2010;4: 107.

32. Sandersius SA, Chuai M, Weijer CJ, Newman TJ. Correlating Cell Behavior with Tissue Topology in Embryonic Epithelia. PLoS ONE. 2011;6: e18081. doi:10.1371/journal.pone.0018081

33. Mao Y, Tournier AL, Hoppe A, Kester L, Thompson BJ, Tapon N. Differential proliferation rates generate patterns of mechanical tension that orient tissue growth. EMBO J. 2013;32: 2790–2803. doi:10.1038/emboj.2013.197

34. Shraiman BI. Mechanical feedback as a possible regulator of tissue growth. Proc Natl Acad Sci U S A. 2005;102: 3318–3323. doi:10.1073/pnas.0404782102

35. Buceta J, Herranz H, Canela-Xandri O, Reigada R, Sagués F, Milán M. Robustness and stability of the gene regulatory network involved in DV boundary formation in the Drosophila wing. PLoS ONE. 2007;2: e602. doi:10.1371/journal.pone.0000602

36. Newman TJ. Modeling multi-cellular systems using sub-cellular elements. ArXivq-Bio0504028. 2005; Available: http://arxiv.org/abs/q-bio/0504028

37. Kursawe J, Brodskiy PA, Zartman JJ, Baker RE, Fletcher AG. Capabilities and Limitations of Tissue Size Control through Passive Mechanical Forces. PLoS Comput Biol. 2015;11: e1004679. doi:10.1371/journal.pcbi.1004679

38. Wartlick O, Mumcu P, Kicheva A, Bittig T, Seum C, Jülicher F, et al. Dynamics of Dpp Signaling and Proliferation Control. Science. 2011;331: 1154–1159. doi:10.1126/science.1200037

39. Fischer-Friedrich E, Hyman AA, Jülicher F, Müller DJ, Helenius J. Quantification of surface tension and internal pressure generated by single mitotic cells. Sci Rep. 2014;4: 6213. doi:10.1038/srep06213

40. Clark AG, Paluch E. Mechanics and Regulation of Cell Shape During the Cell Cycle. In: Kubiak JZ, editor. Cell Cycle in Development. Springer Berlin Heidelberg; 2011. pp. 31–73. Available: http://link.springer.com/chapter/10.1007/978-3-642-19065-0_3

41. Kunda P, Pelling AE, Liu T, Baum B. Moesin Controls Cortical Rigidity, Cell Rounding, and Spindle Morphogenesis during Mitosis. Curr Biol. 2008;18: 91–101. doi:10.1016/j.cub.2007.12.051

42. Lancaster OM, Le Berre M, Dimitracopoulos A, Bonazzi D, Zlotek-Zlotkiewicz E, Picone R, et al. Mitotic Rounding Alters Cell Geometry to Ensure Efficient Bipolar Spindle Formation. Dev Cell. 2013;25: 270–283. doi:10.1016/j.devcel.2013.03.014

43. Guillot C, Lecuit T. Adhesion Disengagement Uncouples Intrinsic and Extrinsic Forces to Drive Cytokinesis in Epithelial Tissues. Dev Cell. 2013;24: 227–241. doi:10.1016/j.devcel.2013.01.010

44. Matzke R, Jacobson K, Radmacher M. Direct, high-resolution measurement of furrow stiffening during division of adherent cells. Nat Cell Biol. 2001;3: 607–610. doi:10.1038/35078583

45. Gibson WT, Veldhuis JH, Rubinstein B, Cartwright HN, Perrimon N, Brodland GW, et al. Control of the Mitotic Cleavage Plane by Local Epithelial Topology. Cell. 2011;144: 427–438. doi:10.1016/j.cell.2010.12.035

46. Buchmann A, Alber M, Zartman JJ. Sizing it up: The mechanical feedback hypothesis of organ growth regulation. Semin Cell Dev Biol. 2014; doi:10.1016/j.semcdb.2014.06.018

47. Hariharan IK. Organ Size Control: Lessons from Drosophila. Dev Cell. 2015;34: 255–265. doi:10.1016/j.devcel.2015.07.012

48. Micoulet A, Spatz JP, Ott A. Mechanical Response Analysis and Power Generation by Single-Cell Stretching. ChemPhysChem. 2005;6: 663–670. doi:10.1002/cphc.200400417

49. Kuznetsova TG, Starodubtseva MN, Yegorenkov NI, Chizhik SA, Zhdanov RI. Atomic force microscopy probing of cell elasticity. Micron. 2007;38: 824–833. doi:10.1016/j.micron.2007.06.011

50. Laurent VM, Kasas S, Yersin A, Schäffer TE, Catsicas S, Dietler G, et al. Gradient of Rigidity in the Lamellipodia of Migrating Cells Revealed by Atomic Force Microscopy. Biophys J. 2005;89: 667–675. doi:10.1529/biophysj.104.052316

51. Sim JY, Moeller J, Hart KC, Ramallo D, Vogel V, Dunn AR, et al. Spatial distribution of cell–cell and cell–ECM adhesions regulates force balance while main-taining E-cadherin molecular tension in cell pairs. Mol Biol Cell. 2015;26: 2456–2465. doi:10.1091/mbc.E14-12-1618

52. Chu Y-S, Thomas WA, Eder O, Pincet F, Perez E, Thiery JP, et al. Force measurements in E-cadherin–mediated cell doublets reveal rapid adhesion strengthened by actin cytoskeleton remodeling through Rac and Cdc42. J Cell Biol. 2004;167: 1183–1194. doi:10.1083/jcb.200403043

579 53. Chiu SN. Aboav-Weaire's and Lewis' laws—A review. Mater Charact. 1995;34: 149–165.
580 doi:10.1016/1044-5803(94)00081-U

581 54. Sanchez-Gutierrez D, Tozluoglu M, Barry JD, Pascual A, Mao Y, Escudero LM.
582 Fundamental physical cellular constraints drive self-organization of tissues. EMBO J. 2015;
583 doi:10.15252/embj.201592374

584 55. Lewis FT. A comparison between the mosaic of polygons in a film of artificial emulsion and
585 the pattern of simple epithelium in surface view (cucumber epidermis and human amnion).
586 Anat Rec. 1931;50: 235–265. doi:10.1002/ar.1090500303

587 56. Aboav DA. The arrangement of grains in a polycrystal. Metallography. 1970;3: 383–390.
588 doi:10.1016/0026-0800(70)90038-8

589 57. Gavet O, Pines J. Activation of cyclin B1-Cdk1 synchronizes events in the nucleus and the
590 cytoplasm at mitosis. J Cell Biol. 2010;189: 247–259. doi:10.1083/jcb.200909144

591 58. Charvin G, Cross FR, Siggia ED. Forced periodic expression of G1 cyclins phase-locks the
592 budding yeast cell cycle. Proc Natl Acad Sci. 2009;106: 6632–6637.
593 doi:10.1073/pnas.0809227106

594 59. Guglielmi G, Barry JD, Huber W, De Renzis S. An Optogenetic Method to Modulate Cell
595 Contractility during Tissue Morphogenesis. Dev Cell. 2015;35: 646–660.
596 doi:10.1016/j.devcel.2015.10.020

597 60. Gibson MC, Patel AB, Nagpal R, Perrimon N. The emergence of geometric order in
598 proliferating metazoan epithelia. Nature. 2006;442: 1038–1041. doi:10.1038/nature05014

599

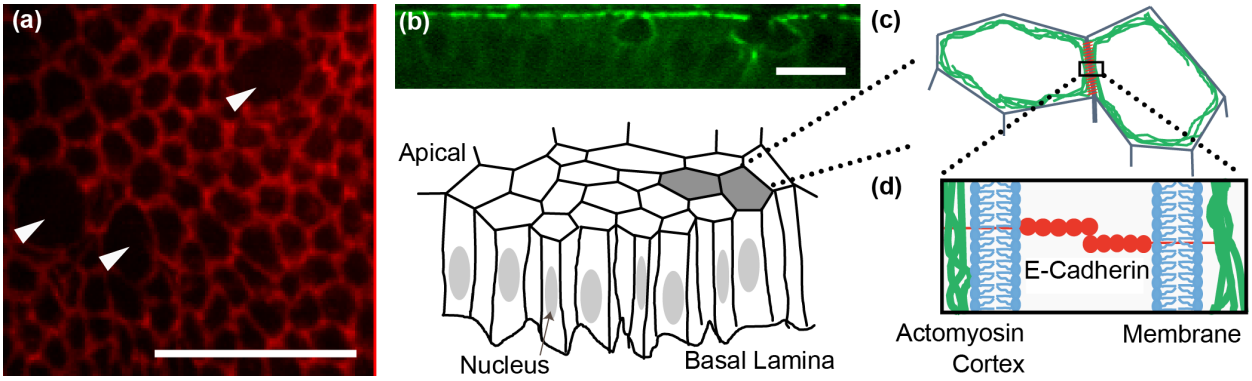

Fig. 1. Epithelial mechanics. (a) Subapical surface of epithelial cells within the *Drosophila* wing imaginal disc that are marked by E-cadherin tagged with fluorescent GFP (DE-cadherin::GFP). Multiple cells within the displayed region are undergoing mitotic rounding. (b) Experimental and cartoon abstraction of epithelial cells, which are polarized with apical and basal sides. Actomyosin and mechanical forces during mitotic rounding are primarily localized near the apical surface. (c) At the molecular scale, the boundary between cells consists of a lipid bilayer membrane for each cell, E-cadherin molecules that bind to each other through homophilic interactions, and adaptor proteins that connect the adhesion complexes to an underlying actomyosin cortex that provides tensile forces along the rim of apical areas of cells. Arrows indicate mitotic cells. Scale bars are 10 micrometers.

614

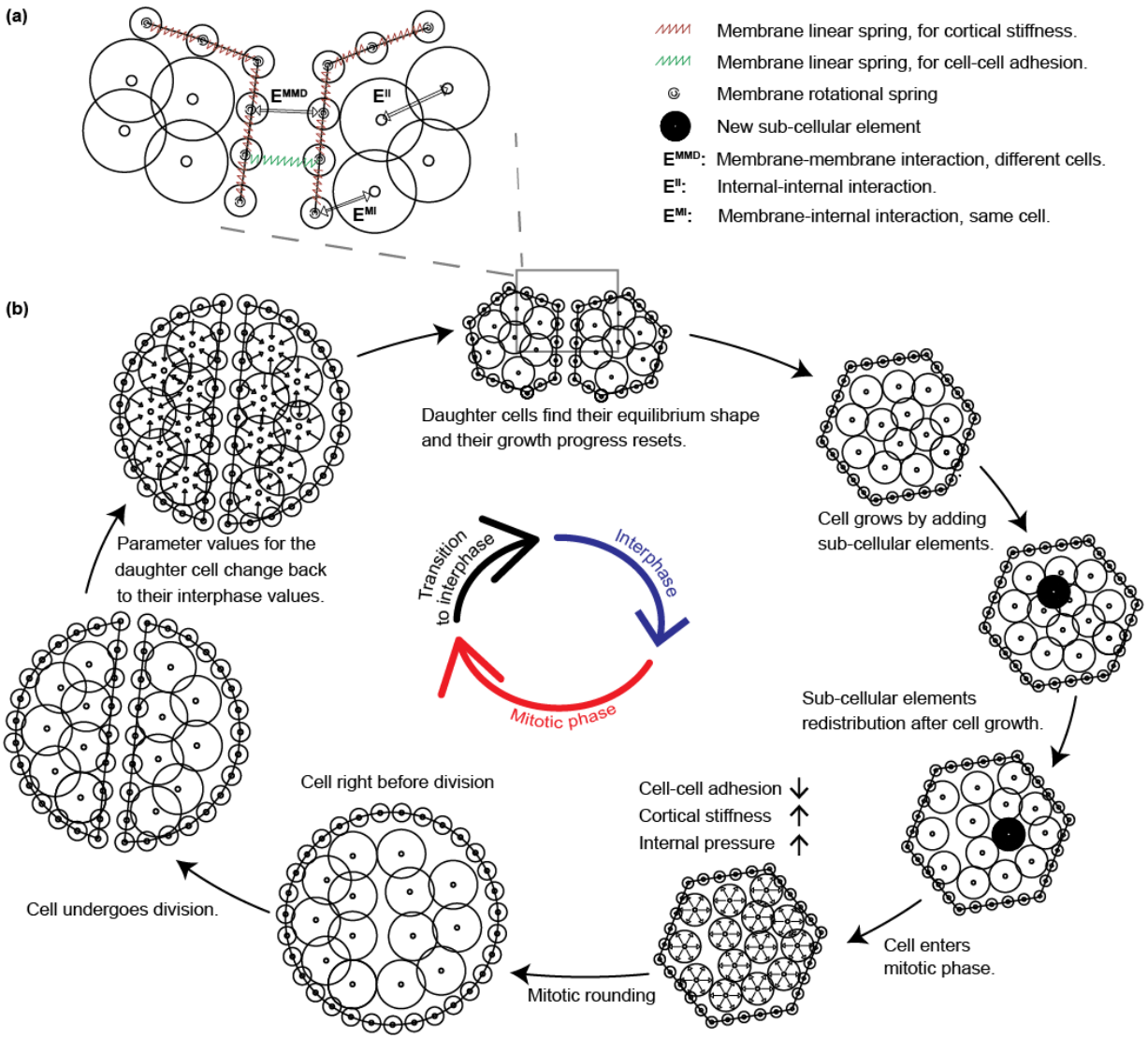

615

616 **Fig. 2**.Diagram of the underlying physical basis of model simulations. (a) Intracellular
617 and intercellular interactions between different elements of the model. (b)
618 Implementation of the simulation of cell cycle in the model.

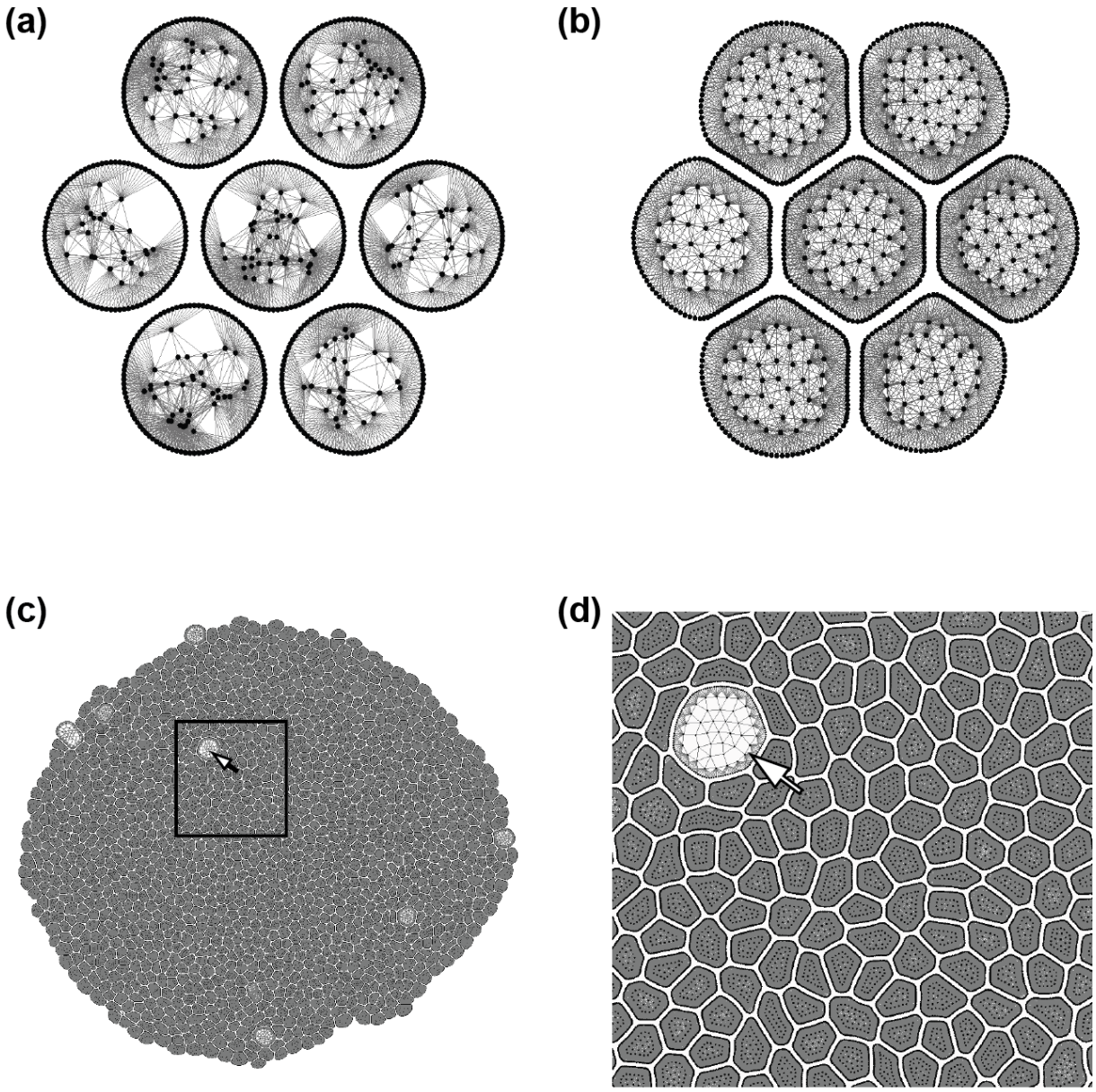

Fig. 3. Initial conditions and sample simulation output. (a) Initial condition of a simulation with seven initially non-adherent circular cells. Each cell starts with 100 membrane elements and 20 internal elements. (b) Initial formation of an epithelial sheet after cells adhere to each other. An equilibrium distribution of internal nodes is reached for each cell. (c) Epithelial sheet after 55 simulated hours of proliferation. (d) Enlarged view of

625 the selected region showing different cell shapes and sizes due to interactions between
626 cells. The large cell is undergoing mitotic rounding (MR). Arrows indicate mitotic cells.

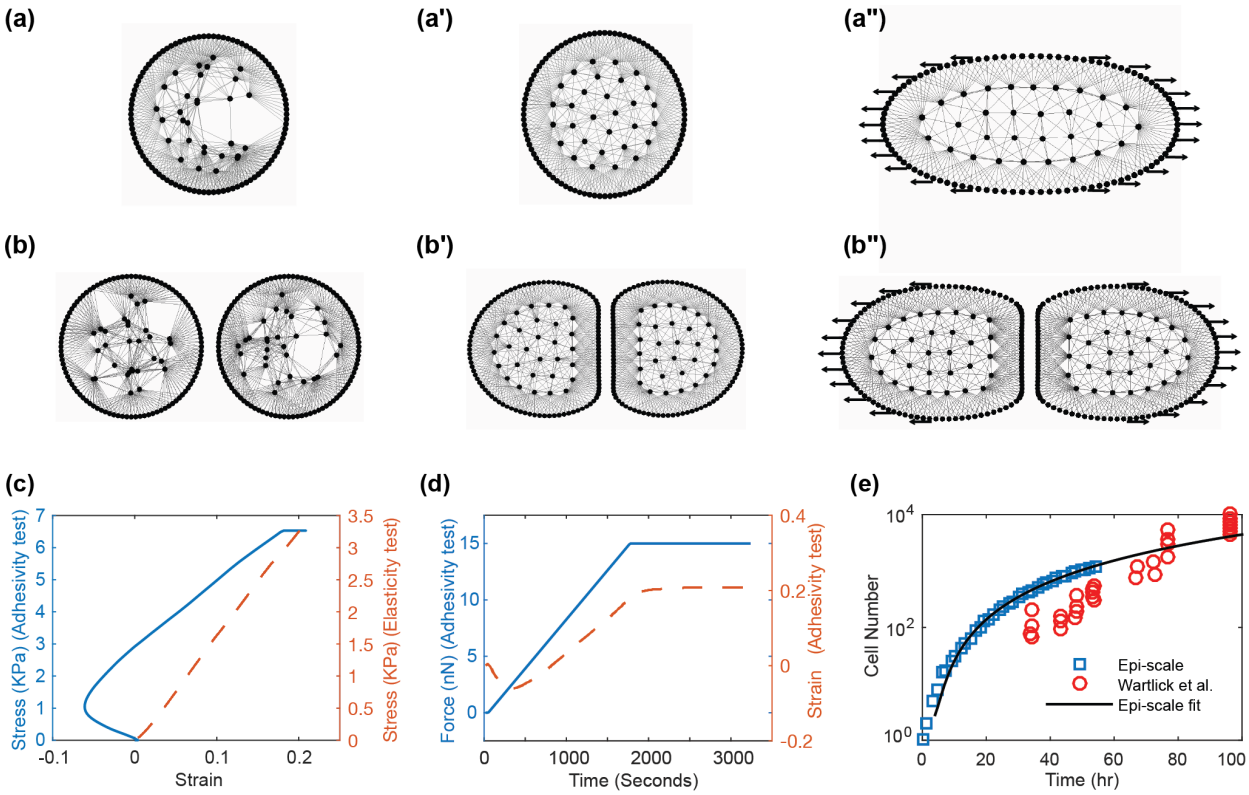

Fig. 4: Calibration of model parameters through simulations. (a-a″) Calibration test to determine parameters for cell elasticity, analogous to experimental single cell stretching tests [48], (a) Initial condition t=0, (a′) 6 minutes after simulation with no force applied, (a″) after 72 minutes cell is completely on tension (b-b″) Cell adhesivity test, analogous to experimental tests [52] for calibrating the level of cell-cell adhesion between adjacent cells. (b) Initial condition t=0, (b′) 6 minutes after simulation begins with no force applied, (b″) after 72 minutes, 15 nN force is applied. (c) Stress versus strain for single cell calibration (red line) and stress versus strain for calibrating the level of adhesivity between the two cells (blue line)[51,52]. Initial negative strain in adhesivity test is due to strong adhesion between two cells. (d) Force and strain as a function of time for adhesivity test. (e) Tissue growth rate calibration by comparing with the experimental data by Wartlick et al. [38].

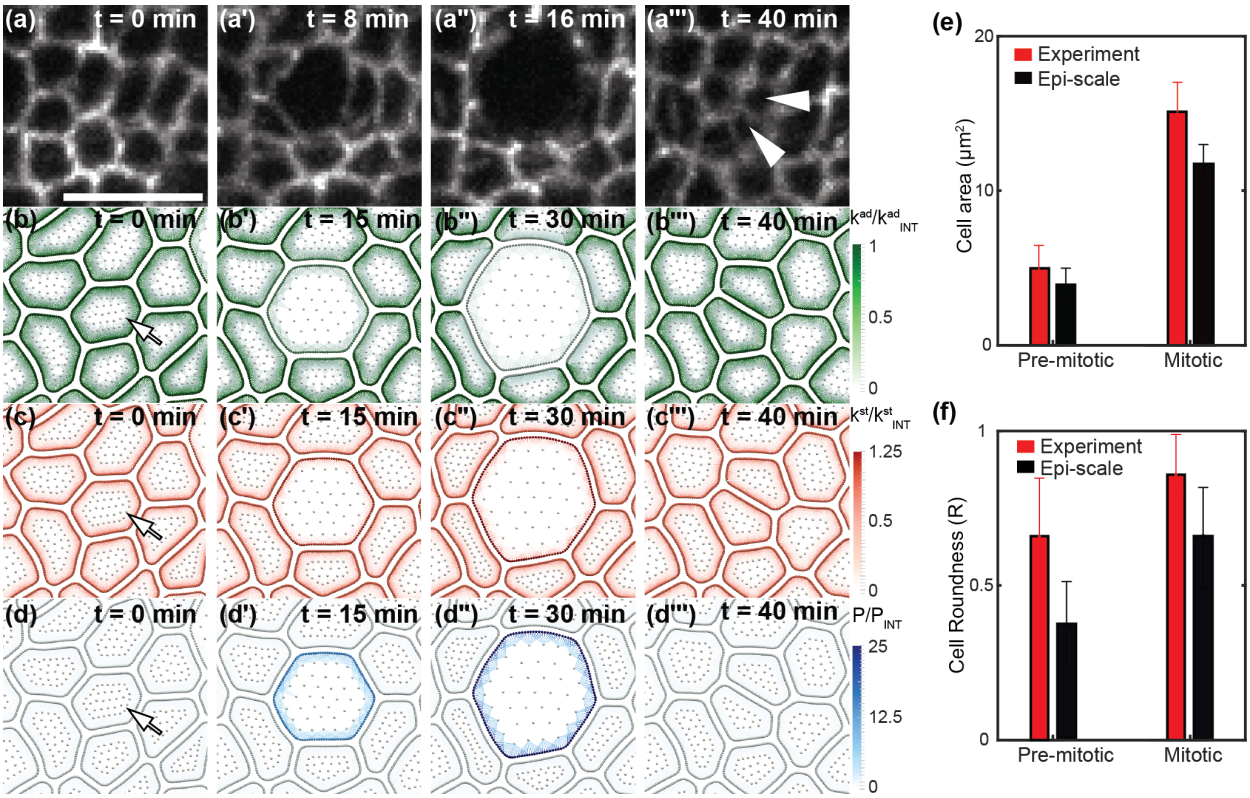

Fig. 5: (a-a"') Time-lapse confocal images of cell undergoing mitosis in the wing disc with E-Cadherin:GFP-labeled cell boundaries. Scale bar is 5 μm. Arrows indicate daughter cells. (b-d"') Time series from Epi-Scale simulation of a cell undergoing mitosis and division with illustration of: (b) adhesive spring stiffness, (c) cortical spring stiffness, and (d) internal pressure, normalized to their interphase values. (e-f) Comparison of size and roundness of mitotic cells with experimental data for the *Drosophila* wing disc. Arrow represents mitotic cell.

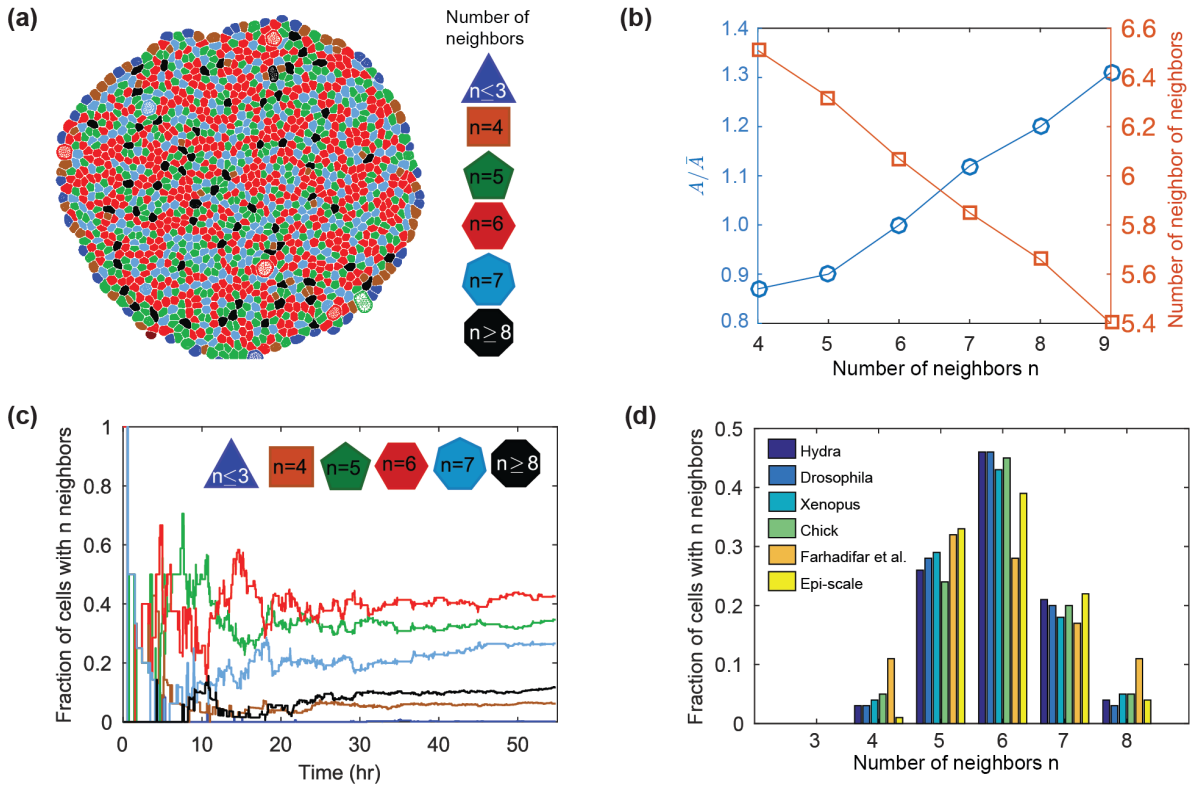

Fig. 6. Emergence of tissue-level statics from model simulations. (a) Sample simulation output showing cells with different numbers of neighbors as different colors (corresponding to legend in b). (b) Average relative area ($\boldsymbol{A/\overline{A}}$) and average polygon class of neighbors for cells of different polygon classes verifying that simulation results follow Lewis law and Aboav-Weaire law. (c) Simulations initiated from seven cells reaches steady-state polygon-class distribution after approximately 35 h of simulated time. (d) Comparison of polygon class distributions obtained by Epi-Scale model with various biological systems (data extracted from [60]) and a vertex based model by Farhadifar et al. [22].

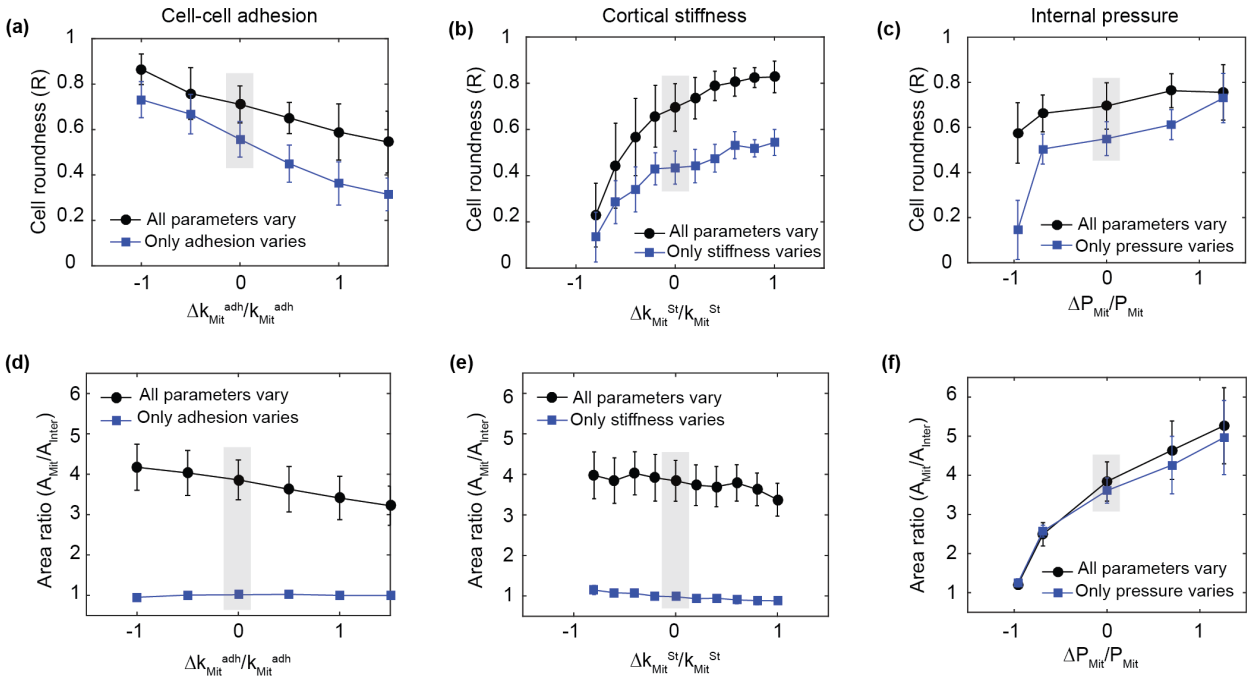

Fig. 7. Predicted sensitivity of MR to perturbations in cell mechanical properties. (a-c) Dependence of roundness (R) on mitotic parameters. Effects of (a) adhesivity between cells, (b) cortical stiffness, and (c) internal pressure on the roundness of the mitotic cells. (d-f) Predicted increase in area during mitosis (A_{Mit}/A_{Inter}). Effects of (d) adhesivity, (e) cortical stiffness, and (f) internal pressure on the roundness of the mitotic cells. The grey shaded region shows the calibrated wild type values for roundness and area ratio when all three parameters are varied (black circles) vs. when only the single parameter is varied (blue squares) during mitosis. P-values of t-tests between the means of cell roundness and area ratio values for single parameter variation and multi-parameter variation are: (a): p=0.068, (b): p =0.0046, (c): p = 0.14, (d): p = $8.7\text{x}10^{-6}$, p = $3.18\text{x}10^{-15}$, p= 0.876.

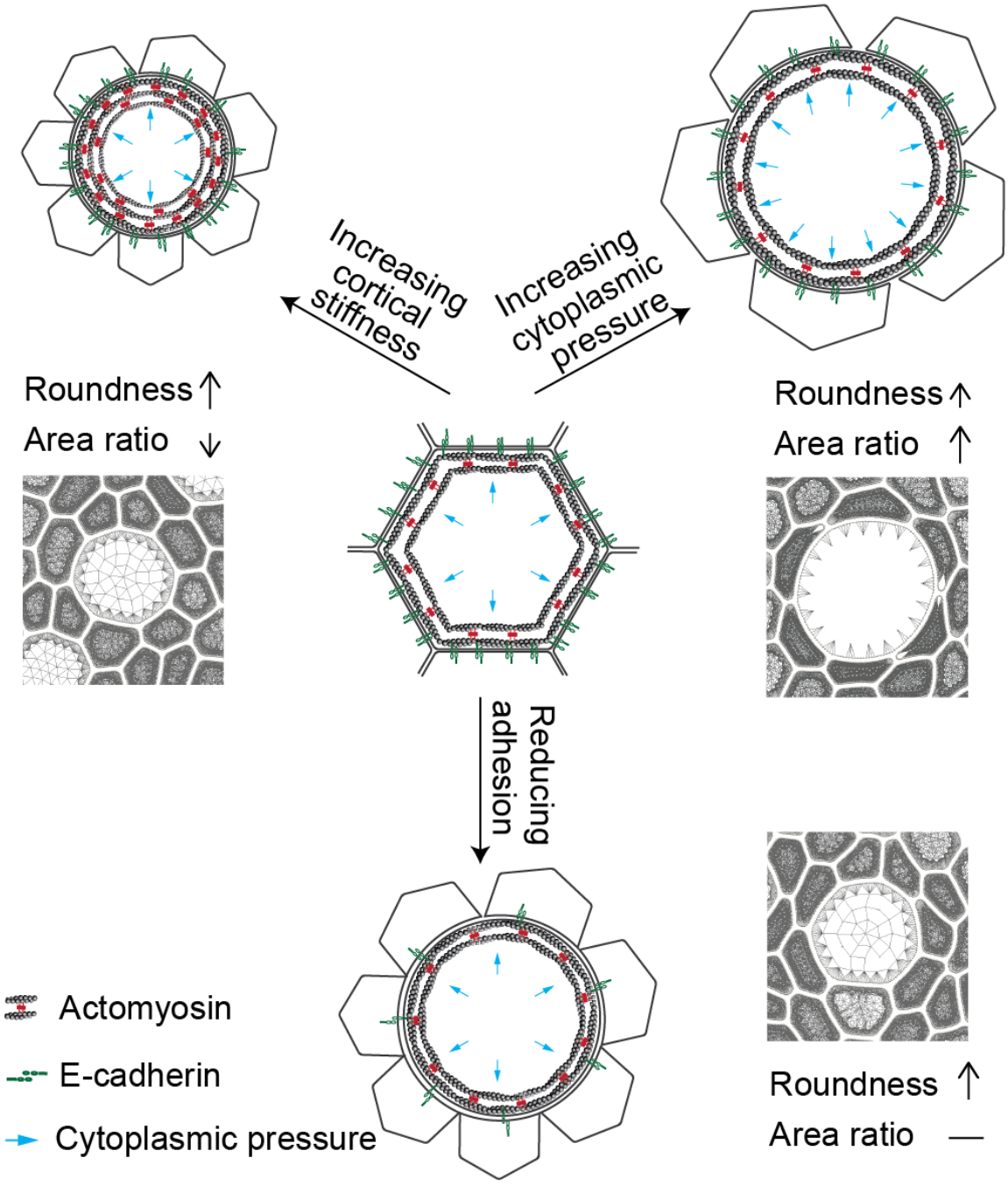

672

673 **Fig. 8.** Schematic detailing the contribution of individual cellular mechanical properties
674 on roundness and size of mitotic cells within constrained tissues as revealed by Epi-
675 Scale simulations. This model extending the graphical model for mitotic rounding
676 presented by Stewart et al.[10] to include the relative effects of each mechanical change
677 in mitotic cells undergoing MR within the constraints of packed tissues.

678 **Table 1:** Potential energy functions in Epi-scale model

Potential function	**Type of potential function**	**Biological concept**
Internal-internal nodes (E^{II}),	Morse	Internal pressure
Membrane-internal nodes (E^{MI})	Morse	Keeps the cytoplasm inside the cell and applies pressure from the cell's cytoplasm to the cell's membrane
Membrane-membrane nodes of neighboring cells (E^{MMD}).	Morse	Prevent membranes of neighboring cells invading into the cell
Membrane-membrane nodes of neighboring cells (E^{adh}).	Linear spring	Adhesion between neighboring cells
Membrane-membrane nodes of the same cell (E^{MMS}).	Linear and torsional spring	Membrane and cortex stiffness of the cell

679

680 **Table 2: Calibrated parameters in Epi-sale**

Parameter	Interphase	Mitotic phase	Values during interphase & mitosis	Source
E^{II}	U_{Inter}^{II}	U_{Mit}^{II}	0.488 & $19\ nN.\mu m$	Matched to experimental data (SI-Appendix S3)
	W_{Inter}^{II}	W_{Mit}^{II}	0.146 & $5.86\ nN.\mu m$	
	ξ_{Inter}^{II}	ξ_{Mit}^{II}	0.3125& $0.54\ \mu m$	
	γ_{Inter}^{II}	γ_{Mit}^{II}	$1.25\ \mu m$	
E^{MI}	U_{Inter}^{MI}	U_{Mit}^{MI}	0.78 & $3.81\ nN.\mu m$	Boundary condition
	ξ_{Inter}^{MI}	ξ_{Mit}^{MI}	0.125 & $0.25\ \mu m$	
E^{MMD}	U_{Inter}^{MMD}	U_{Mit}^{MMD}	$3.91\ nN.\mu m$	Boundary condition
	W_{Inter}^{MMD}	W_{Mit}^{MMD}	$3.91\ nN.\mu m$	
	ξ_{Inter}^{MMD}	ξ_{Mit}^{MMD}	$0.125\ \mu m$	
	γ_{Inter}^{MMD}	γ_{Mit}^{MMD}	$1.5625\ \mu m$	
E^{adh}	k_{Inter}^{adh}	k_{Mit}^{adh}	20 & $8\ nN/\mu m$	[43,51,52]
	L_{adh}	L_{adh}	$0.2\ \mu m$	
E^{MMS}	k_{Inter}^{St}	k_{Mit}^{St}	200 & $250\ nN/\mu m$	[49,50]
	L_{Inter}^{St}	L_{Mit}^{St}	0.06 & $0.125\ \mu m$	
	L_{Inter}^{RSt}	L_{Mit}^{RSt}	6 & $7\ nN.\mu m/rad$	

681

682 ** Other Morse parameters are equal to zero.

683

684 **Table 3:** Tissue scale parameters in Epi-scale

Parameter	Value	Reference
η	$36\ nN.s/\mu m$	[38]
$g_{0_{min}}$ & $g_{0_{max}}$	2×10^{-3} & $4\times10^{-3} P/s$	[38]
k_g	$4\times10^{-4}\ 1/s$	[38]

685

686 **Table 4: Impact of adhesion, stiffness, and cytoplasmic pressure on MR**

Fig. panels	**Adhesion in Mitotic phase**	**Cortical stiffness in M phase**	**Pressure in M phase**	**Total variation of roundness***	**Total variation of A_{Mit}/A_{Inter}***
Fig. 7a, 7d (Blue line)	varied	same as interphase	same as interphase	-0.42	0.04
Fig. 7b, 7e (Blue line)	same as interphase	varied	same as interphase	0.41	-0.26
Fig. 7c, 7f (Blue line)	same as interphase	same as interphase	varied	0.58	4.69
Fig. 7a, 7d (Black line)	varied	same as wild type	same as wild type	-0.32	-0.95
Fig. 7b, 7e (Black line)	same as wild type	varied	same as wild type	0.59	-0.60
Fig. 7c, 7f (Black line)	same as wild type	same as wild type	varied	0.18	4.69

687

688

689 *These values are reported based on varying the desired parameter from 100% below the

690 calibrated value to 100% above the calibrated value